Slowing hot-electron relaxation in mix-phase nanowires for hot-carrier photovoltaics

Journal:	*Nano Letters*
Manuscript ID	nl-2021-02725g.R2
Manuscript Type:	Communication
Date Submitted by the Author:	n/a
Complete List of Authors:	Wang, Hailu; Shanghai Institute of Technical Physics, State Key Laboratory of Infrared Physics Wang, Fang; Shanghai Institute of Technical Physics Xu, Tengfei; Shanghai Institute of Technical Physics, State Key Laboratory of Infrared Physics Xia, Hui; Shanghai Institute of Technical Physics, Chinese Academy of Sciences, National Laboratory for Infrared Physics Xie, Runzhang; Shanghai Institute of Technical Physics, State Key Laboratory of Infrared Physics Zhou, Xiaohao; Shanghai Institute of Technical Physics Ge, Xun; East China Normal University Liu, Weiwei; Shanghai Institute of Technical Physics, State Key Laboratory of Infrared Physics Zhu, Yicheng; Shanghai Institute of Technical Physics, State Key Laboratory of Infrared Physics Sun, Liaoxin; Shanghai Institute of Technical Physics, National Lab for Infrared Physics Guo, Jiaxiang; Shanghai Institute of Technical Physics, State Key Laboratory of Infrared Physics Ye, Jiafu; Shanghai Institute of Technical Physics, State Key Laboratory of Infrared Physics Zubair, Muhammad; Shanghai Institute of Technical Physics, State Key Laboratory of Infrared Physics Luo, Man; Nantong University Yu, Chenhui; Nantong University Sun, Deyan; East China Normal University, Physics Li, Tianxin; Shanghai Institute of Technical Physics, Chinese Academy of Sciences, National Laboratory for Infrared Physics Zhuang, Qiandong; Lancaster University, Fu, Lan; ANU Research School of Physics and Engineering, Hu, Weida; Shanghai Institute of Technical Physics, Chinese Academy of Sciences, National Lab for Infrared Physics Lu, Wei; Shanghai Insitute of Technique Physics,

Slowing hot-electron relaxation in mix-phase nanowires for hot-carrier photovoltaics

Hailu Wang[1,8†], Fang Wang[1,8†], Tengfei Xu[1,6†], Hui Xia[1,8], Runzhang Xie[1,8], Xiaohao Zhou[1,8], Xun Ge[1,5], Weiwei Liu[1,8], Yicheng Zhu[1,8], Liaoxin Sun[1,8], Jiaxiang Guo[1,8], Jiafu Ye[1,8], Muhammad Zubair[1,8], Man Luo[4], Chenhui Yu[4], Deyan Sun[5], Tianxin Li[1,8], Qiandong Zhuang[2], Lan Fu[3], Weida Hu[1,8*], Wei Lu[1,7,8*]*

[1]State Key Laboratory of Infrared Physics, Shanghai Institute of Technical Physics, Chinese Academy of Sciences, 500 Yutian Road, Shanghai 200083, China

[2]Department of Physics, Lancaster University, Lancaster LA1 4YB, UK

[3]Department of Electronic Materials Engineering, Research School of Physics, The Australian National University, Canberra, ACT 2601, Australia

[4]Jiangsu Key Laboratory of ASIC Design, School of Information Science and Technology, Nantong University, Nantong 226019, China

[5]Department of Physics, East China Normal University, Shanghai 200241, China

[6]Frontier Institute of Chip and System, Fudan University, Shanghai 200438, China

[7]School of Physical Science and Technology, ShanghaiTech University, Shanghai 201210, China.

[8]University of Chinese Academy of Sciences, Beijing 100049, China

*Corresponding author: huix@mail.sitp.ac.cn (H. Xia); wdhu@mail.sitp.ac.cn (W. Hu); luwei@mail.sitp.ac.cn. (W. Lu)

†H. Wang, F. Wang, and T. Xu contributed equally to this work.

Abstract

Hot carrier harvest could save 30% energy loss in solar cells. So far, however, it is still unreachable as the photo-excited hot carriers are short-lived, ~1 ps, determined by a rapid relaxation process, thus invalidating any reprocessing efforts. Here we propose and demonstrate a feasible route to reserve hot electrons for efficient collection. It is accomplished by an intentional mix of cubic zinc-blend and hexagonal wurtzite phases in III-V semiconductor nanowires. Additional energy levels are then generated above the conduction band minimum, capturing and storing hot electrons before they cool down to the band edges. We also show the superiority of core/shell nanowire (radial heterostructure) in extracting hot electrons. Strategy disclosed here may offer a unique opportunity to modulate hot carriers for efficient solar energy harvest.

Keywords: mix-phase nanowire, hot electrons, InAs, radial heterostructure, photovoltaics

Introduction

In Shockley-Queisser theory, the efficiency of solar cells is limited to 33% but not 66% owing to a huge waste of hot-carrier energies [1,2]. Generally, the energetic electrons and holes, generated by absorbing high-energy photons, quickly (~1 ps) cool down to the band edges. It is accompanied by a large number of phonon emissions, leading to a 30-40% energy loss [3-7]. Given this effect, attention has been focused on the hot-carrier reserve technique which subsequently gives rise to the concept of hot-carrier photovoltaics [8-17]. Particularly, two different routines were carefully examined. One is to introduce quantum structures into photovoltaic devices [18-20]. In such a strategy, the spatial confinement effect leads to a discrete distribution of energy levels (rather than a continuous distribution as in bulk material), the gap of which is much higher than the phonon energy. In this way, the phonon emissions are highly suppressed (phonon bottleneck) and the hot-carriers life is then significantly prolonged. The other possibility is to make use of the upper

satellite bands for the temporary storage of hot carriers [21-23]. In the conduction band of III-V semiconductor, for example, there are L and X valleys besides the bottom Γ valley, which have the potential to hold hot electrons with low energy loss. As great efforts are paid on these routes, the device applications, however, are still challenging. Specifically, the spectral response deviates from the solar spectrum, and the efficiency of hot carrier extraction is low [19,23].

In this work, we propose and demonstrate a distinct approach for hot-carriers harvest. It is realized by an intentional mix of cubic zinc-blend and hexagonal wurtzite phases in III-V semiconductor nanowires. Additional upper energy bands are then generated above the conduction band minimum, capturing and retaining hot electrons during their relaxing downward process. To extract these hot electrons (through visible illumination), we design a core/shell nanowire heterostructure to facilitate the radial transport of the hot electrons. At the same time, cold electrons (through infrared illumination) are collected in the axial direction. Findings disclosed here may provide a unique perspective on hot carrier management for future high-efficiency solar cells.

Results and Discussion

The sun's radiation closely matches that of a black body at 5800 K (Figure 1b), which shows a wide spectral distribution, from visible (300-700 nm) to infrared (700-2500 nm) bands, with the proportion of ~46% and ~54%, respectively. For a solar cell, to harvest or respond to the whole spectral radiation, the bandgap of the absorption layer should be below 0.5 eV [5]. However, few photovoltaic structures follow the idea. Because there is a deep carrier relaxation/cooling process in low bandgap material, which will not only waste the optical profit (gained from a broadband light absorption) but also leads to an additional energy loss [1,2]. Therefore, there is the paradox: more colorful lights absorbed, more energies lost (see detailed discussion in Supplementary Section 2).

Figure 1a shows a distinct route to address such a problem. It is based on the reconstruction of the semiconductor band structure that potentially harvests visible and infrared lights independently in a single material. Specifically, the interband transition, with an energy gap below 0.5 eV, is attributed to harvest infrared lights, from 700-2500 nm wavelength. Additionally, an extra band is artificially constructed, locating at ~1 eV above the conduction band, for capturing and storing hot electrons that are generated by absorbing visible lights (300-700 nm wavelength). To that end, we highlight the mix-phase III-V semiconductor and its role in multi-stage light harvesting. Typically,

the cubic zinc-blend (ZB) phase is the dominated crystal structure in III-V bulk materials, whereas a mix of hexagonal wurtzite (WZ) and cubic zinc-blend phases is frequently found in their confined system, like nanowire [24-26]. Such character allows us to conveniently prepare the test sample, e.g., a mix-phase InAs nanowire sample assembled by the molecular beam epitaxy (MBE) method. Figure 2a shows its high magnification annular dark-field image. There are a stacking sequence of one-monolayer (1L) WZ/1L ZB/2L WZ InAs segments in the field of vision, thus a proportion of 25% ZB and 75% WZ, respectively. Statistics on a much wider area give a floating value for ZB phase mixing from 25% to 50%, more in Supplementary Figure S2.

To show how mix-phase structures alter the band structure of InAs, we performed the first-principles calculations with Vienna Ab-initio Simulation Package using the projector augmented wave method (details in Supplementary Section 1) [27,28]. Pure WZ and 25% ZB phase structures (Figure 2a) are calculated for comparison, with the corresponding density-of-states distributions (versus energy) depicted in Figure 2b. Obviously, the ZB-phase mixture introduces upper states located at 0.8-1.1 eV above the conduction band minimum. Those additional states are expected to act as a reservoir that captures and retains hot electrons (generated by absorbing visible photons) during their relaxing downward process, as schematically shown in Figure 2c.

Worth noting that efforts have been paid on the energy band structure of WZ/ZB mix-phase semiconductors, where the WZ and ZB segments were treated as two distinct materials; the whole structure was then taken as superlattice or type II heterostructure [29-31]. The model is well accepted for understanding the below-bandgap transition process observed in luminescent experiments. However, the possibility of treating a mix-phase structure as a single semiconductor is barely discussed in previous works. The idea is reasonable since there are no other elements but In and As (in this study), more importantly, all the In-As bonds are identical to each other and no apparent discontinuity or interstitial was observed between monolayers.

Figure 3b shows the photoluminescence spectrum of a assemble of mix-phase InAs nanowires. Apart from the interband transition peaked at the infrared band (@3306 nm/0.375 eV, referring to our previous work Ref. 32), one can find a weak visible light luminescence that is peaked at 760 nm (a Lorentzian fit of the spectra identifies two other features located at 780 and 820 nm, Figure 2b.). It indicates that there is an above-bandgap transition process, that could span from the valence-band-maximum to some energy levels of ~1.46 eV higher. Such high energy levels might be mix-phase associated levels (MPALs) since their energies are very close to the predictions (1.0-1.3 eV above the conduction band).

Photoelectric measurements could provide further information on the energy band structure. Figure 3a schematically shows the single InAs nanowire device structure, where InAs nanowire (with ~60 nm in diameter and ~5 μm in length) was physically transferred onto the Si substrate capped with a 300 nm SiO_2 layer, following by electron-beam lithography, thermal evaporation, and lift-off processes to define the electrode patterns (details in Supplementary Section 1). Technically, incident photons, with energies varying from 0.8 to 2.76 eV, were taken as a probe to visualize the energy gap and charge carrier dynamic process. Typical results (@77 K) are shown in Figure 3c. For infrared-light irradiation ($\lambda \geq 785$ nm, $h\upsilon \leq 1.58$ eV), the mix-phase InAs nanowire behaves appropriately as a semiconductor, that is characterized by an enhanced conductance. One can also find an increasing photoresponse with the increase of light wavelength. It arises from a simple fact that the photon number is inversely proportional to the photon energy while the global energy remains unchanged (~3 mW). Of particular interest is that the mix-phase InAs nanowire responds negatively to the visible lights (decline in conductance). Considering that once the photocarriers relax to the band edges, they are energetically leveling and thus contribute equally and positively to the conductance. Therefore, changes must occur in the photocarrier dynamic/relaxation process when the illumination switches from infrared to visible lights.

With this in mind, we focus on the photocarrier dynamic process. The transition point occurs at λ≈730 nm (Figure 3c and Supplementary Figure S6) when the photoconductance changes from positive to negative (More details in Supplementary Section 5. The transition point between individuals is somewhat different, ranging from 720-830 nm. It might account for the wide range of luminescence observed in a assemble of nanowires, Figure 3b). At this specific region, the electrons are photoexcited to energy levels of ~1.48 eV above the valence band maximum (Figure 2c), which highly coincides with the MPALs (~1.46 eV, Figure 2b and 3b). Thus, it is reasonably believed that the negative photoresponse is associated with those high-energy states. Here we propose a model to understand such a distinct photoelectric process. As schematically shown in Figure 2c, the hot electrons, generated by absorbing visible lights, are captured and stored in those MPALs during their relaxing downward process. As a consequence, the photo-excited holes recombine with the background doping electrons, leading to an enormous reduction in the conductance/carrier concentration. The infrared illumination will be a quite different situation, where the photo-excited electrons are far below the MPALs thus relax to the conduction band minimum without any barriers.

Further experiments confirm such a physical image. Figure 3d shows the dependence of the negative photoresponse on the illumination intensity (More details in Supplementary Figure S4). Clearly, an ultra-high light intensity would lower the negative photoresponse. It is reasonable since the MPALs are fully filled; part of hot electrons is capable of relaxing downward (Figure 2c). In this case, a rising positive photoresponse starts to neutralize the negative signal. Such character also explains why the photoresponse of 637 nm laser is lower than that of 450 and 520 nm case (Figure 3c, more visible photons under the same illumination intensity).

Slowing hot-carrier cooling is not the destination. In this section, we demonstrate a feasible route to efficiently collect hot electrons. For this purpose, we additionally grow a 5-10 nm AlSb capping layer for InAs nanowire (more details in Supplementary Section 6), with the band-alignment depicted in Figure 4b [33]. Under visible illumination, the generated hot electrons are first captured by the MPALs of the InAs core and then directed to the AlSb shell by the built-in electric field. As stated above (Figure 2c), axial transport of hot carriers is highly suppressed in mix-phase InAs nanowire, probably due to the low mobility at MPALs. In the radial direction, however, the orders of magnitude reduction in transit distance make it possible to harvest them. Figure 4a schematically shows the device structure and preparation process. InAs/AlSb core/shell nanowire is physically

transferred onto Si/SiO_2 substrate. Chromium/gold (Cr/Au, 15/60 nm) electrode was first fabricated onto one end, enabling an electric contact to the AlSb shell. Then, a chemical process, with 2% HF solution for ~5 s, was performed to remove the rest capping layer (except those protected by the electrode). After that, two other electrodes were fabricated on the InAs core. Such three-terminal devices make sure that we can independently test the photoelectric performance of mix-phase-InAs solely and AlSb/mix-phase-InAs radial heterostructure.

Figure 4c shows the dark and photoexcited I_{ds}-V_{ds} curves of InAs solely and AlSb/InAs heterojunction. Interestingly, the AlSb/InAs heterojunction shows a confident positive photoresponse, in contrast to the negative photoconductance of the InAs conductor. Considering that the AlSb layer is buried under a 75 nm metal electrode, light absorbed there is thus negligible. In other words, there is no difference in photogeneration between the two devices, both taking place at InAs core. Thus, the transition (of the polarity of photoresponse) must come from the charge-carrier transport. More specifically, it should arise from an efficient collection of hot carriers. If not, the residual hot carriers will still serve as negative gate-bias in depleting the core region. Another interesting sign is that there is an obvious photovoltaic voltage in AlSb/InAs heterojunction, which could be solid evidence for the interfacial separation/collection of hot

electrons (more experiment details are shown in Supplementary Figure S9 to eliminate the possibility of non-ohmic contact formed on AlSb [34]).

In this radial heterojunction architecture, the transmit distance is taken as 30 nm, two orders of magnitude less than that in the axial direction (>1 μm). The lifetime (τ) needed for the hot-electrons extraction can be roughly estimated by the equation as follows [35]:

$$L = \sqrt{D * \tau} = \sqrt{\frac{\mu k_B T}{q} * \tau},$$

where L=30 nm is the diffusion length, D is the diffusion coefficient, μ=~15 $cm^2V^{-1}s^{-1}$ is the mobility (derived by an estimate of the transfer characteristic of the nanowire, more details in Supplementary Section 4), k_B is the Boltzmann constant, T is the temperature, and q is the elementary charge. Thus, the lifetime should be at least 23 ps. It implies that hot-electrons life might be several tens of picoseconds in the mix-phase nanowire. Also, it reflects a harsh reality for traditional solar cells, in which the absorption layer (micrometer in thickness) is too long for hot carriers to transit through even they are artificially prolonged to a maximum of ~100 ps [18,36-39]. Considering this effect, we highlight core-shell nanowire and its application in hot carrier solar cells. Naturally, the light absorption (along axial direction) and carrier separation paths (along

radial direction) are decoupled, which offers an opportunity to collect hot carriers in their diffusion length.

In summary, this work proposes and demonstrates a distinct route for hot carriers harvest in III-V semiconductors. It is featured by an intentional mix of wurtzite and zinc-blende phases that give rise to energy levels locating at ~1.4 eV above the conduction band minimum. During the carrier relaxation process, those high energy levels capture hot electrons and give them a sufficiently prolonged life to be extracted by a radial nanowire heterostructure. Such characteristic might offer an opportunity to develop hot carrier solar cells, where the intrinsic energy band harvests cold carriers (generated by absorbing infrared lights), the artificially constructed band helps to collect hot carriers (by absorbing visible lights, a detailed discussion of such architecture is depicted in Supplementary Section 7).

Supporting information

Section 1, experimental methods of nanowire devices; Section 2, quantitative interpretation of the relationship between bandgap and energy loss; Section 3, high-resolution annular dark-field image; Section 4, transfer characteristic curves at room temperature; Section 5, power-dependent spectral response; Section 6, additional experimental data of the radial nanowire heterostructure; Section 7, a detailed discussion of the potential structure for mix-phase-nanowire hot-carrier solar cells.

Funding

This work was supported by National Natural Science Foundation of China (Grant No. 11991063, 62004207, 62074085, and 62104118), International Partnership Program of Chinese Academy of

Sciences (Grant No. 181331KYSB20200012), Royal Society-Newton Advanced Fellowship (Grant No. NA170214), Shanghai Science and Technology Committee (Grant No. 18JC1420401 and 20YF1455900), Special Research Assistant Grant from the Chinese Academy of Sciences Foundation (Grant No. 2019-169), Strategic Priority Research Program of Chinese Academy of Sciences (Grant No. XDB43010200) and Youth Innovation Promotion Association of the Chinese Academy of Sciences.

Author Contributions

H. Xia, W. Hu, and W. Lu proposed the idea, designed the experiments and supervised the project. H. Wang, F. Wang, and T. Xu contributed equally to this work. H. Xia and H. Wang analyzed the data and prepared the manuscript. H. Wang fabricated nanowire devices and performed all the measurements. X. Ge, D. Sun, and X. Zhou performed the DFT calculation. W. Liu carried out the FDTD simulation. Q. Zhuang synthetized nanowire materials. Y. Zhu and L. Sun helped to perform the PL spectra measurements. J. Guo, J. Ye, M. Zubair, and M. Luo helped to prepare nanowire devices. C. Yu, T. Li, and L. Fu discussed and commented on the manuscript.

Author Information

Corresponding Author

*H. X.: E-mail: huix@mail.sitp.ac.cn.
*W. H.: E-mail: wdhu@mail.sitp.ac.cn.
*W. L.: E-mail: luwei@mail.sitp.ac.cn.

ORCID

Hailu Wang: 0000-0002-6771-7677
Hui Xia: 0000-0002-3150-0505
Liaoxin Sun: 0000-0003-4769-3388
Deyan Sun: 0000-0002-9728-8017
Lan Fu: 0000-0002-9070-8373
Weida Hu: 0000-0001-5278-8969

Conflict of interest statement. None declared.

References

1. Shockley, W.; and Queisser, H. J. Detailed Balance Limit of Efficiency of p-n Junction Solar Cells. *Journal of Applied Physics* **1961**, 32, 510-519.
2. Ross, R. T. and Nozik, A. J. Efficiency of hot-carrier solar energy converters. *Journal of Applied Physics* **1982**, 53, 3813-3818.

3. Polman, A. and Atwater, H. A. Photonic design principles for ultrahigh-efficiency photovoltaics. *Nature Materials* **2012**, 11, 174-177.
4. Wolf, M. Limitations and possibilities for improvement of photovoltaic solar energy converters. *Proc. IRE* **1960**, 48, 1246-1263.
5. Green, M. A. *Third Generation Photovoltaics: Advanced Solar Energy Conversion*; Springer-Verlag Berlin Heidelberg, 2003; pp 69-72.
6. Wong, J.; Jariwala, D.; Tagliabue, G.; Tat, K.; Davoyan, A. R.; Sherrott, M. C.; Atwater, H. A. High photovoltaic quantum efficiency in ultrathin van der waals heterostructures. *ACS Nano* **2017**, 11, 7230-7240.
7. Jariwala, D.; Davoyan, A. R.; Wong, J.; Atwater, H. A. Van der waals materials for atomically-thin photovoltaics: promise and outlook. *ACS Photonics* **2017**, 4, 12, 2962-2970.
8. Guo, Z.; Wan, Y.; Yang, M.; Snaider, J.; Zhu, K. and Huang, L. Long-range hot-carrier transport in hybrid perovskites visualized by ultrafast microscopy. *Science* **2017**, 356, 59-62.
9. Zhu, H.; Miyata, K.; Fu, Y.; Wang, J.; Joshi, P.; Niesner, D.; Williams, K.; Jin, S. and Zhu, X. Screening in crystalline liquids protects energetic carriers in hybrid perovskites. *Science* **2016,** 353, 1409-1413.
10. Li, M.; Fu, J.; Xu, Q. and Sum, T. C. Slow Hot-Carrier Cooling in Halide Perovskites: Prospects for Hot-Carrier Solar Cells. *Adv. Mater.* **2018**,1802486.
11. König, D.; Casalenuovo, K.; Takeda, Y.; Conibeer, G.; Guillemoles, J. F. and Patterson, R. Hot carrier solar cells: principles, materials and design. *Physica. E: Low-dimensional Systems and Nanostructures* **2010**, 42, 2862-2866.
12. Nozik, A. J. Utilizing hot electrons. *Nature Energy* **2018**, 3, 170-171.
13. Nguyen, D. T.; Lombez, L.; Gibelli, F.; Boyer-Richard, S.; Corre, A. L. Durand, O. Quantitative experimental assessment of hot carrier-enhanced solar cells at room temperature. *Nature Energy* **2018**, 3, 236-242.
14. Green, M. A. and Bremner, S. P. Energy conversion approaches and materials for high-efficiency photovoltaics. *Nature Materials* **2016**, 16, 23-34.
15. Conibeer, G. Shrestha, S.; Huang, S.; Patterson, R.; Xia, H.; Feng, Y.; Zhang, P.; Gupta, N.; Tayebjee, M.; Smyth, S.; Liao, Y.; Lin, S.; Wang, P.; Dai, X. and Chung, S.Hot carrier solar cell absorber prerequisites and candidate material systems. *Sol. Energ. Mater. Sol. C.* **2015**,

135, 124-129.

16. Tregnago, G. Electrons stay hot. Nature Energy **2018**, 3, 1021.
17. Gold-Parker, A.; Gehring, P. M.; Skelton, J. M.; Smith, I. C.; Parshall, D.; Frost, J. M.; Karunadasa, H. I.; Walsh, A. and Toney, M. F. Acoustic phonon lifetimes limit thermal transport in methylammonium lead iodide. *Proc. Natl Acad. Sci. USA* **2018**, 115, 11905-11910.
18. Li, M.; Bhaumik, S.; Goh, T. W.; Kumar, M. S.; Yantara, N.; and Grtzel, M. Slow cooling and highly efficient extraction of hot carriers in colloidal perovskite nanocrystals. *Nature Communications* **2017**, *8*, 14350.
19. Tisdale, W. A.; Williams, K. J.; Timp, B. A.; Norris, D. J.; Aydil, E. S. and Zhu, X. Y. Hot-electron transfer from semiconductor nanocrystals. *Science* **2010**,328, 1543-1547.
20. Ye, Y.; Ostrowski, D. P.; France, R. M.; Kai, Z.; Lagemaat, J. and Luther, J. M. Observation of a hot-phonon bottleneck in lead-iodide perovskites. *Nature Photonics* **2016**, *10*, 53.
21. Clady, R.; Tayebjee, M.; Aliberti, P.; König, D. and Green, M. A. Interplay between the hot phonon effect and intervalley scattering on the cooling rate of hot carriers in GaAs and InP. *Prog. Photovolt.* **2012**, 20, 82-92.
22. Whiteside, V. R.; Esmaielpour, H.; Mishima, T. D.; Dorman, K. R.; Santos, M. B.; Ferry, D. K. and Sellers, I. R. The role of intervalley scattering in hot carrier transfer and extraction in type-II InAs/AlAsSb quantum well solar cells. *Semicond. Sci. Technol.* **2019**, 34, 094001.
23. Esmaielpour, H.; Dorman, K. R.; Ferry, D. K.; Mishima, T. D.; Santos, M. B.; Whiteside, V. R. and Sellers, I. R. Exploiting intervalley scattering to harness hot carriers in Ⅲ-Ⅴ solar cells. *Nature Energy* **2020**, 5, 336-343.
24. Galicka, M.; Bukała, M.; Buczko, R. and Kacman, P. Modelling the structure of GaAs and InAs nanowires. *J. Phys.: Condens. Matter* **2008**, 20, 454226.
25. Hjort, M.; Lehmann, S.; Knutsson, J.; Zakharov, A. A.; Du, Y. A.; Sakong, S.; Timm, R.; Nylund, G.; Lundgren, E.; Kratzer, P.; Dick, K. A. and Mikkelsen, A. Electronic and structural differences between wurtzite and zinc blende InAs nanowire surfaces: experiment and theory. *ACS Nano* **2014**, 8, 12346-55.
26. Zhang, Z.; Liu, N.; Li, L.; Su, J.; Chen, P. P. and Lu, W. In situ TEM observation of crystal structure transformation in InAs nanowires on atomic scale. *Nano Letters* **2018**, 18, 6597-6603.

27. Kresse, G.; Furthmüller, J., Efficient iterative schemes for ab initio total-energy calculations using a plane-wave basis set. *Physical Review B* **1996**, 54, 11169-11186.
28. Blöchl, P. E. Projector augmented-wave method. *Physical Review B* **1994**, 50, 17953-17979.
29. Vainorius, N.; Jacobsson,D.; Lehmann, S.; Gustafsson, A.; Dick, K. A.; Samuelson, L. and Pistol, M. Observation of type-II recombination in single wurtzite/zinc-blende GaAs heterojunction nanowires. *Physical Review B* **2014**, 89, 165423.
30. Heiss, M.; Conesa-Boj, S.; Ren, J.; Tseng, H. H.; Gali, A.; Rudolph, A.; Uccelli, E.; Peiro´, F.; Morante, J. R.; r Schuh, D.; Reiger, E.; Kaxiras, E.; Arbiol, J. and Morral, A. F. I. Direct correlation of crystal structure and optical properties in wurtzite/zinc-blende GaAs nanowire heterostructures. *Physical Review B* **2011**,83, 045303.
31. Spirkoska, D.; Arbiol, J.; Gustafsson, A.; Conesa-Boj, S. and Morral, A. F. Structural and optical properties of high-quality zinc-blende/wurtzite GaAs nanowire heterostructures. *Physical Review B* **2009**, 80, 245325.
32. Li, H.; Alradhi, H.; Jin, Z.; Anyebe, E. A.; Sanchez, A. M. and Linhart, W. M. Novel type-Ⅱ InAs/AlSb core-shell nanowires and their enhanced negative photocurrent for efficient photodetection. *Advanced Functional Materials* **2017**,1705382.
33. Nakagawa, A.; Kroemer, H. and English, J. H. Electrical properties and band offsets of InAs/AlSb n-N isotype heterojunctions grown on GaAs. *Appl. Phys. Lett.* **1989**, 54, 1893.
34. Jariwala, D.; Davoyan, A. R.; Tagliabue, G.; Sherrott, M. C.; Wong, J.; Atwater, H. A. Near-unity absorption in van der waals semiconductors for ultrathin optoelectronics. *Nano Lett.* **2016**, 16, 5482-5487.
35. Sze, S. M.; Ng, K. K. *Physics of Semiconductor Devices*; John Wiley & Sons, **2006**; pp 62-68.
36. Yang, Y.; Ostrowski, D. P.; France, R. M.; Zhu, K.; Lagemaat, J.; Luther, J. M. and Beard, M. C. Observation of a hot-phonon bottleneck in lead-iodide perovskites. *Nat. Photonics* **2016**, 10, 53-59.
37. Zhu, H.; Miyata, K.; Fu, Y.; Wang, J.; Joshi, P. P.; Niesner, D.; Williams, K. W.; Jin, S. and Zhu, X.-Y. Screening in crystalline liquids protects energetic carriers in hybrid perovskites. *Science* **2016**, 353, 1409.
38. Niesner, D.; Zhu, H.; Miyata, K.; Joshi, P. P.; Evans, T. J. S.; Kudisch, B. J.; Trinh, M. T.; Marks, M. and Zhu, X.-Y. Persistent Energetic Electrons in Methylammonium Lead Iodide

Perovskite Thin Films. *J. Am. Chem. Soc.* **2016**, 138, 15717-15726

39. Chang, A. Y.; Cho, Y.; Chen, K.; Chen, C.; Kinaci, A.; Diroll, B. T.; Wagner, M. J.; Chan, M. K. Y.; Lin, H. and Schaller, R. D. Slow Organic-to-Inorganic Sub-Lattice Thermalization in Methylammonium Lead Halide Perovskites Observed by Ultrafast Photoluminescence. *Adv. Energy Mater.* **2016**, 6, 1600422.

Figure captions

Figure 1. Energy band tailoring towards hot carrier solar cells. Left panel: band structure of an artificially constructed three-level system. The blue and red arrows indicate the optical absorption processes from valence band maximum (VBM) to artificially constructed extra band (ACEB) and conduction band minimum (CBM), respectively. The black arrows represent the hot-electrons relaxation processes. The gap of the VBM-CBM and VBM-ACEB are designed to ~0.5 and ~1.5 eV for the light absorption of infrared (700-2500 nm) and visible (300-700 nm) light, respectively. Right panel: standard solar spectrum of AM1.5G (International standard: ISO 9845-1-1992). The blue (orange) background shows the visible (infrared) lights component of solar spectrum radiation.

Figure 2. Principle of storing hot electrons. (a) Crystal structures of mix-phase InAs nanowire. Top panel: high magnification annular dark-field image showing mixed wurtzite and zinc-blend phases structure (one-monolayer (1L) WZ/1L ZB/2L WZ: 25% ZB phases). Scale bar: 1 nm. Bottom panel: schematic of mix-phase InAs with 25% ZB phases (3L WZ/1L ZB) in DFT calculation. The green and purple balls represent In and As atoms, respectively. (b) Simulated density-of-states (DOS) of pure WZ and 25% ZB phase structures for InAs. (c) Dynamic and kinetic processes of charge carriers transport in mix-phase InAs nanowire device. High/low injection represents the strong/weak illumination power intensity. First column: hot carriers freely relax down to the band edges under infrared lights illumination. The blue (red) wave line represents the visible (infrared) light. The green (orange) balls represent electrons (holes). The black arrows show hot-carriers relaxation processes. Second column: all hot electrons, generated by weak visible lights illumination, are captured by the mix-phase associated levels (MPALs). By contrast, the excess-holes recombine with the background doping electrons (marked by a black dotted rectangle). Third column: MPALs are full-filled upon a high-level photo-injection condition of visible lights. In return, part of the hot electrons relaxes to the band edges.

Figure 3. Photoelectric properties of mix-phase InAs nanowire. (a) Schematic of the nanowire transistor. (b) Photoluminescence spectra of a assemble of mix-phase InAs nanowire with the excitation of 532 nm laser. The plot is fitted by three Lorentzian peaks at 760, 780, and 820 nm, respectively. Inset: illustration of the transition processes in the nanowire. (c) Dependence of photoresponse on the excitation wavelength at 77 K. Additionally, a gate-bias of -20 V is applied to recover the nanowire conductance after visible illumination. (d) Dependence of current flow on illumination power. The excitation wavelength is 450 nm and the working temperature is kept at 77 K.

Figure 4. Hot-electrons harvest through radial nanowire heterojunction. (a) Schematic illustrating the preparation process for the AlSb/mix-phase InAs nanowire radial heterostructure. Left panel: InAs/AlSb nanowire with one Cr/Au electrode contacted with AlSb shell. Middle panel: chemical treatment process to remove the rest capping layer (except those protected by the electrode). Right panel: InAs nanowire and AlSb/InAs heterostructure device. Bias-voltage is applied to the middle common-electrode (contacted with InAs) while the two other ends are kept ground. (b) Band

alignment of the AlSb/mix-phase InAs nanowire radial heterostructure. The blue (red) arrow shows the light absorption in the visible (infrared) range. The hot electrons excited by the visible light are captured by the mix-phase associated levels and then transferred to the AlSb shell layer. (c) Dark and photoexcited (λ= 450 nm) I-V curves of mix-phase InAs (left panel) and AlSb/mix-phase InAs nanowire (right panel) devices at room temperature.

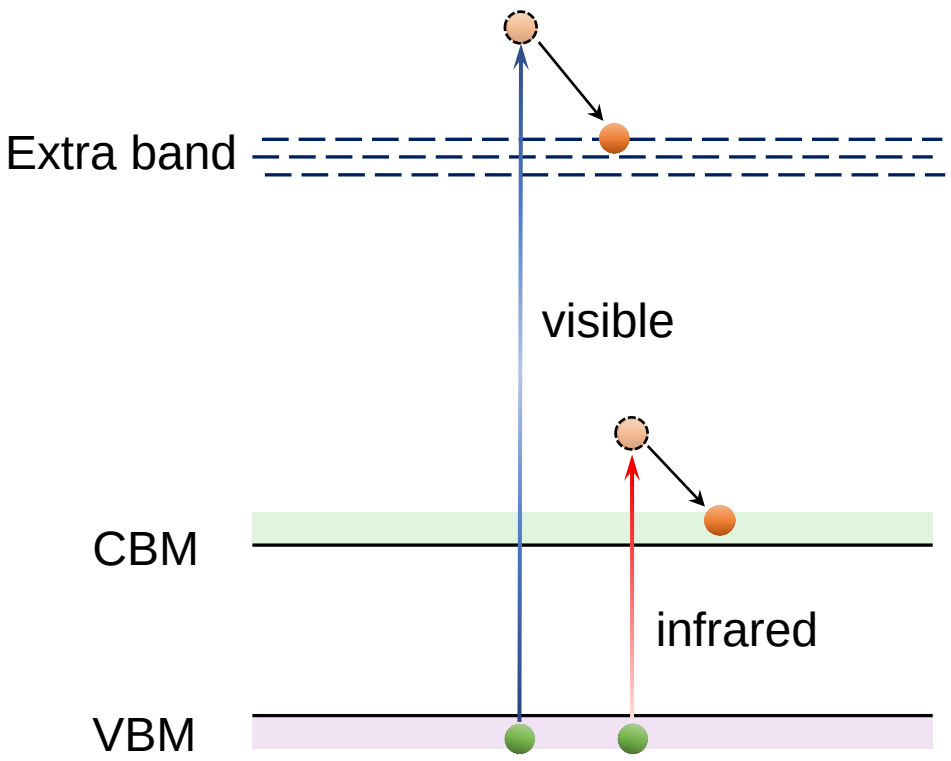
Extra band
visible
CBM
infrared
VBM

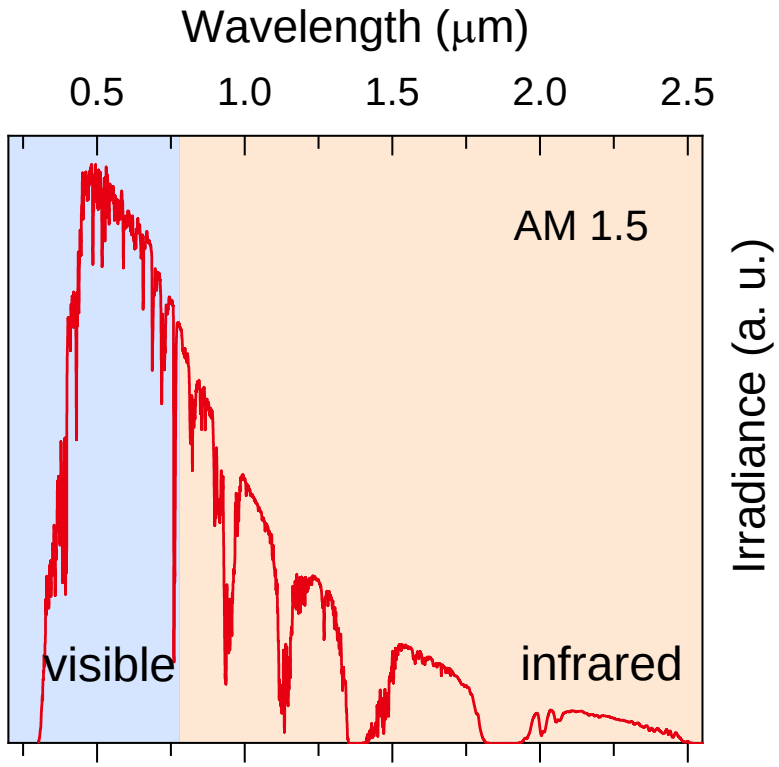
Wavelength (μm)
0.5
1.0
1.5
2.0
2.5
AM 1.5
visible
infrared
Irradiance (a. u.)

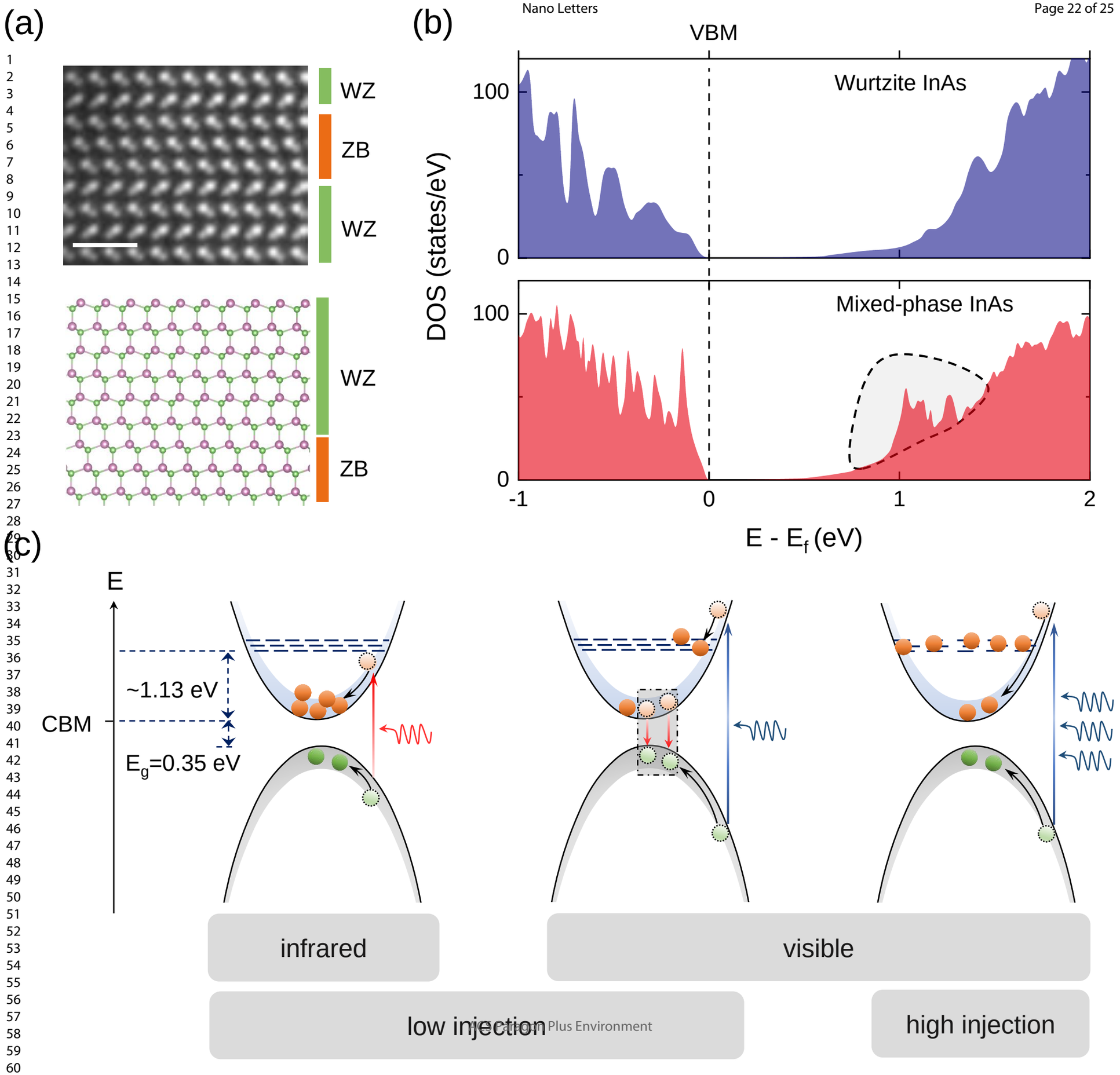

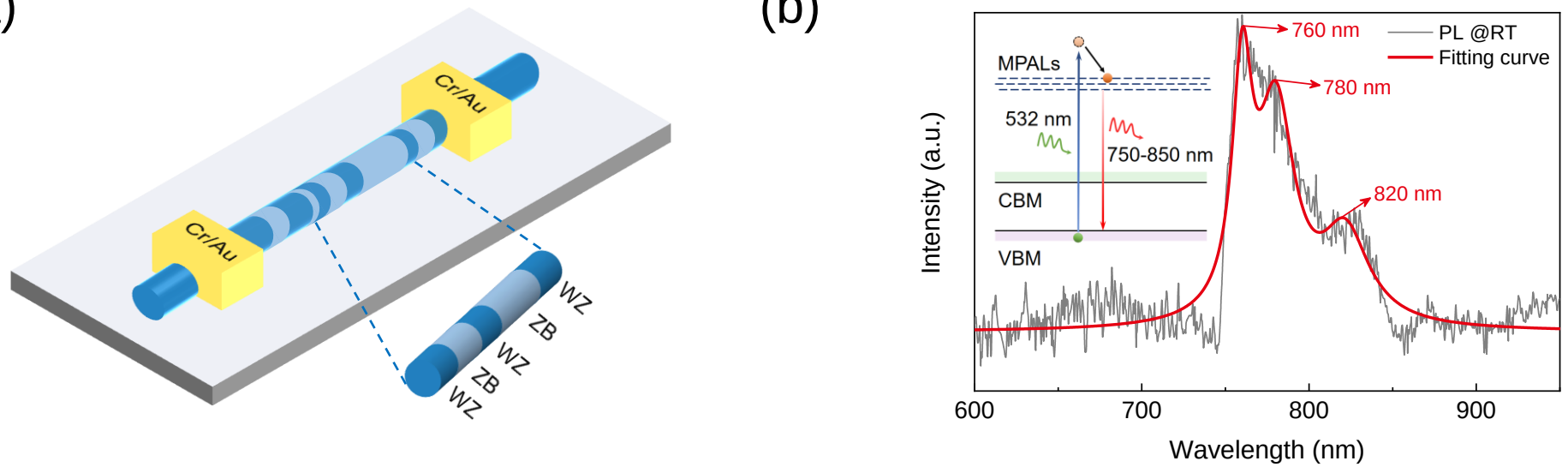
(a)
Cr/Au
Cr/Au
WZ
ZB
WZ
ZB
WZ
(b)
MPALs
532 nm
750-850 nm
CBM
VBM
760 nm
780 nm
820 nm
PL @RT
Fitting curve
Intensity (a.u.)
600
700
800
900
Wavelength (nm)
(c)
P (mW)
λ=450
520
637
785
830
1550 nm
3
0
V_g (V)
0
-20
2
0
Net photocurrent (× 100 nA)
@77 K
Time (a.u.)
(d)
P
dark
0.6 μW
1.6 μW
2.8 μW
1.6 mW
3.5 mW
4.2 mW
λ=450 nm
10^{-7}
10^{-8}
10^{-9}
Current (A)
@77 K
0
40
80
120
Time (s)

(a)

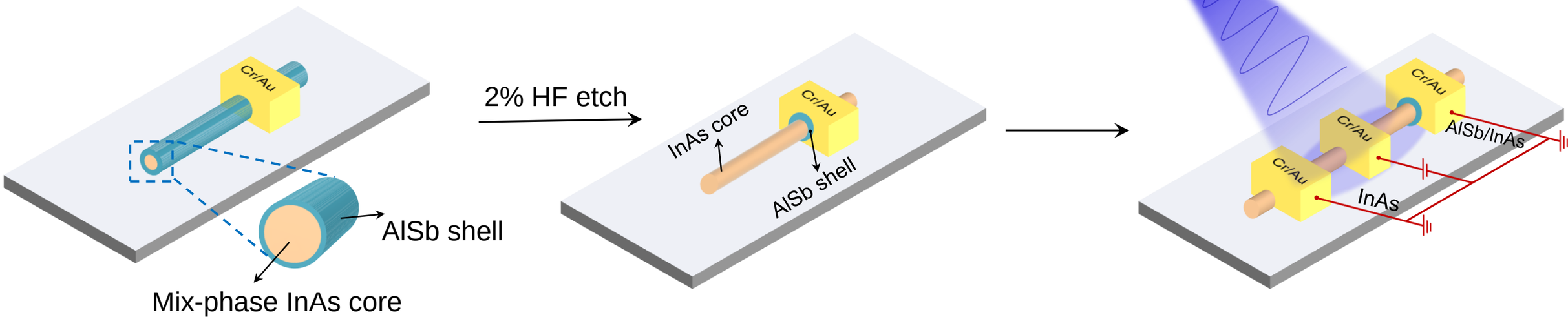
Cr/Au
AlSb shell
Mix-phase InAs core
2% HF etch
InAs core
Cr/Au
AlSb shell
Cr/Au
Cr/Au
Cr/Au
AlSb/InAs
InAs

(b)

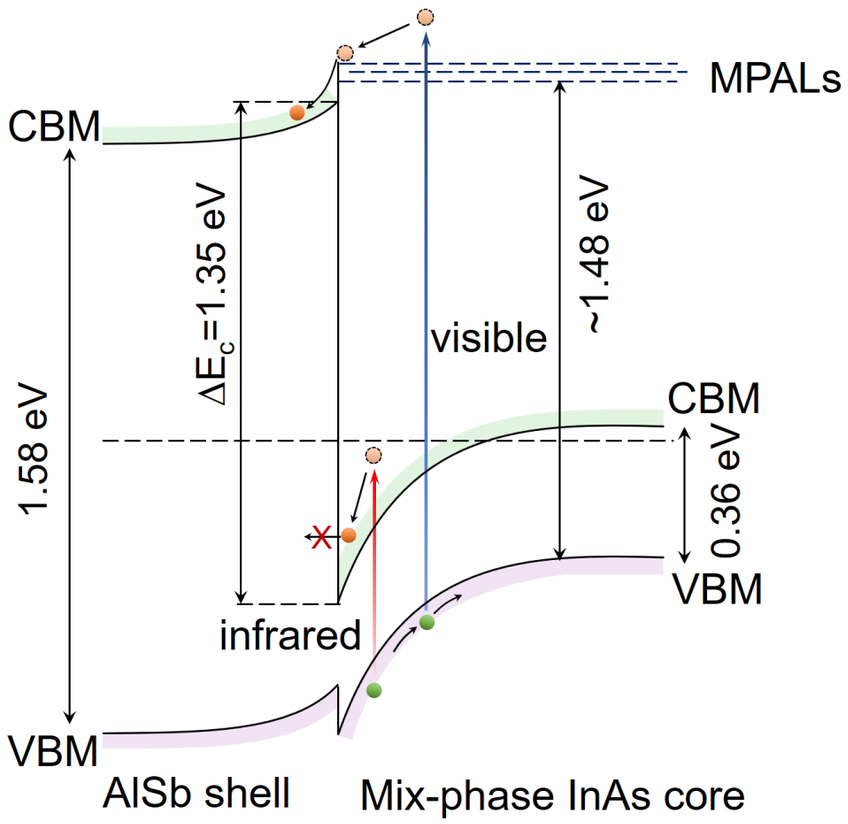
MPALs
CBM
ΔEc=1.35 eV
visible
~1.48 eV
1.58 eV
CBM
0.36 eV
VBM
infrared
VBM
AlSb shell
Mix-phase InAs core

(c)

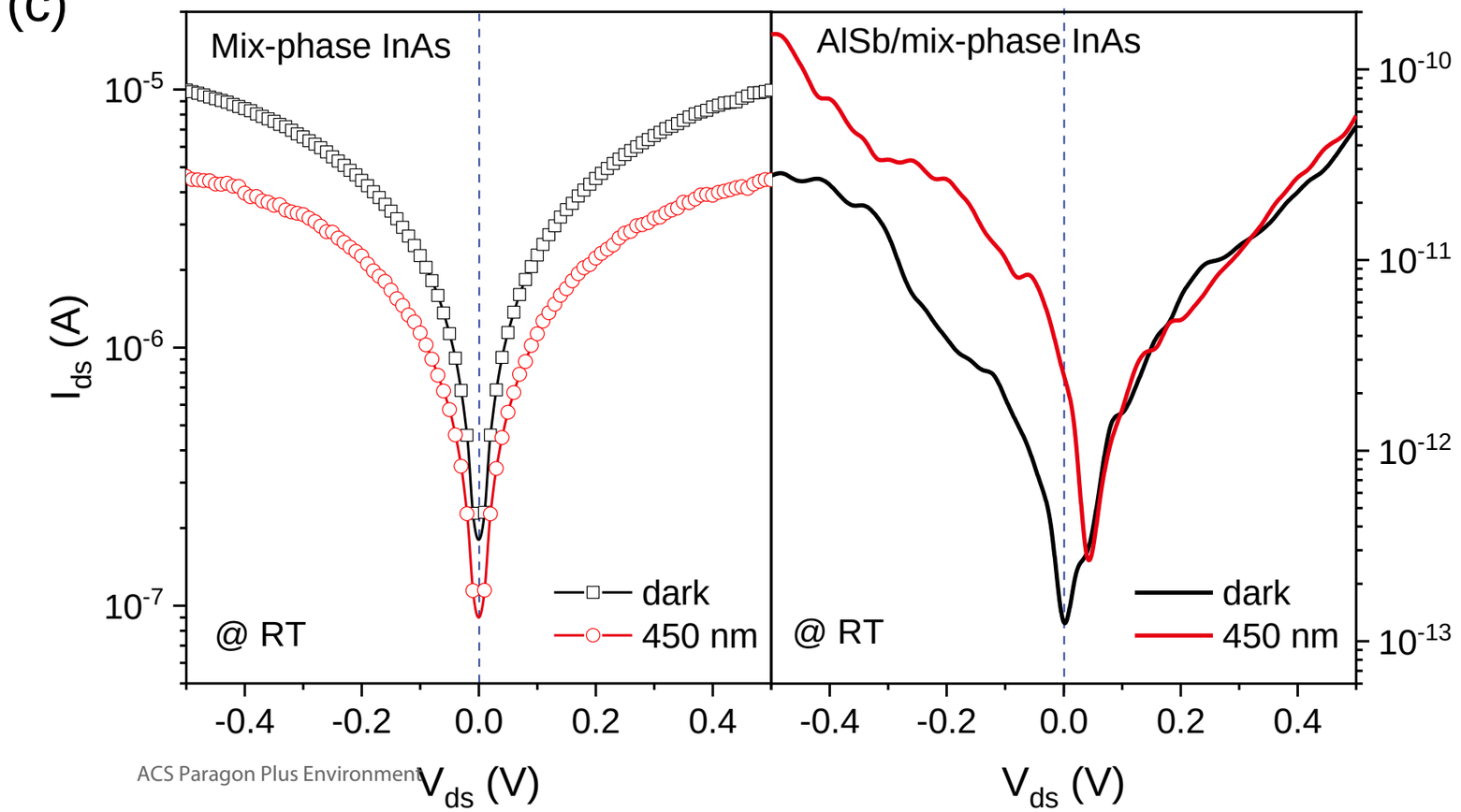
Mix-phase InAs
AlSb/mix-phase InAs
10-5
10-6
10-7
Ids (A)
10-10
10-11
10-12
10-13
dark
450 nm
@ RT
dark
450 nm
@ RT
-0.4
-0.2
0.0
0.2
0.4
-0.4
-0.2
0.0
0.2
0.4
Vds (V)
Vds (V)

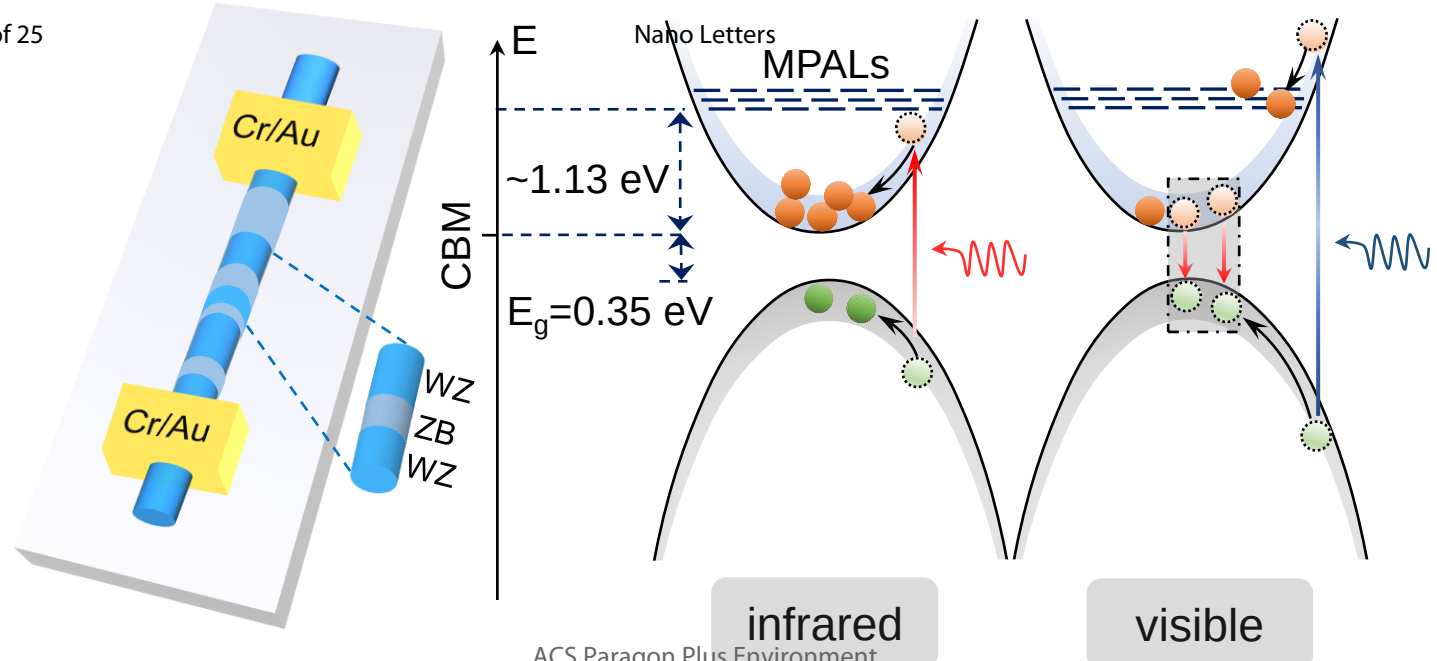

ACS Paragon Plus Environment

TOC graphic